 CMES, vol.24, no.3, pp.203-213, 2008

Effects of Dopants on the Mechanical Properties of Nanocrystalline Silicon Carbide Thin Film

Liming Xiong[1] **and Youping Chen**[1]

Abstract: This paper presents the application of an atomistic field theory (AFT) in modeling and simulation of boron- , boron/nitrogen and silicon/nitrogen-doped nanocrystalline silicon carbide (B-, BN-, SiN-SiC). Intergranular glassy films (IGFs) and nano-sized pores have been obtained in triple junctions of the grains in nanocrystalline SiC (nc-SiC). Residual tensile stress in the SiC grains and compressive stress in the grain boundaries (GBs) are observed. Under uniaxial tension, the constitutive responses of nanocrystalline SiC were reproduced from the simulations. It is found that the mechanical properties of nanocrystalline SiC are strongly dependent on the compositions of GBs. Although there are more nano-sized pores in the triple junctions of the grains, interestingly, compared with B-Si and BN-SiC, SiN-SiC exhibits the highest strength. Numerically, for crystalline materials, it has been shown that AFT can be naturally reduced to atomic-level simulation when the finite element meshes is reduced to the network of lattice.

Keyword: nanocrystalline ceramics, silicon carbide, atomistic field theory, dopants

1 Introduction

The structure and mechanical behavior of nanocrystalline materials, i.e., polycrystalline materials with a grain size of typically less than about 100 nm, has been the subject of considerable interest ever since polycrystalline metals with a grain size of less than 0.1 micrometer were first synthesized in bulk about 20 years ago. In contrast with nanostructured metals, the great interest in nanostructured ceramics has been originating from the observations of unique properties such as very high hardness, high fracture toughness and superplastic behavior in normally brittle ceramics.

In particular, silicon carbide (SiC) ceramics have been of interest because of their potential technological applications in high-temperature structural and electronic components (Madar, 2004). As high-temperature materials, SiC ceramics offer many advantages including high melting temperatures, low density, high elastic modulus and strength, and good resistance to creep, oxidation and wear. However, its application to date has been severely limited by its poor fracture toughness properties. Recently, experiments have shown that its toughness is essentially determined by soft (often amorphous) grain boundary phase (Chen, 2000) and its hardness is sensitive to the grain size and the fraction of the amorphous grain boundary phase (Liao, 2005). Low inherent fracture toughness of conventional SiC ceramics has been improved by producing a composite, typically accomplished by incorporating second-phase particles such as aluminum, boron or carbon (Chen, 2000). Second phase effects on the grain boundary structure, cyclic-fatigue properties and abrasive wear behavior of the Aluminum-Boron-Carbon-Silicon carbide has been investigated through HRTEM (Zhang, 2001, 2003). Compression deformation mechanism of fine-grained Boron- and Carbon-doped silicon carbide has been revealed through SEM (Shinnoda, 2004). Different from ABC-SiC ceramics toughened by containing aluminum, boron and carbon as sintering additives, the microstructures in SiC with rare-earth or aluminum oxide additions has been analyzed by image analysis, crack deflection has been observed (Zhou,2001;Kim,2007). Moreover, while maintaining superhard and su-

[1] Department of Mechanical and Aerospace Engineering, University of Florida, Gainesville, Florida, 32611

perbrasive properties, nanostructured diamond-SiC composites with enhanced fracture toughness have been synthesized (Zhao, 2004). It is seen that the reported experimental results have suggested that the mechanical properties of the conventional SiC ceramics can be improved by optimizing the intergranular-phase chemistry through judicious selection of sintering additives. Experimental advance on nanocrystalline ceramics has created a concurrently need for a quantitative and predictive understanding, and posed a great challenge to theoretical study that can predict, tailor and optimum design nanostructured ceramics.

Theoretical investigations and simulations of mechanical properties of nanostructured ceramics have taken on special significance. Pioneering simulation work has been done for covalent single crystal materials (Tang and Yip, 1994, 1995; Keblinsky, 1996). Recently, in nano-indentation testing simulation, multimillion-atom molecular dynamics (MD) simulations of nanocrystalline silicon carbide (nc-SiC) have predicted a crossover from intergranular continuous deformation to intragrain discrete deformation at a critical indentation depth (Szlufarska, 2005). In the simulation of tensile testing, MD simulations performed on nc-SiC have shown that reduction of grain size promote simultaneous enhancement of ductility, toughness, and strength. It was also found that nc-SiC failed by intergranular fracture preceded by atomic level necking (Mo and Szlufarska, 2007). At room temperature, the atomic configurations, vibration spectra, and stress-strain curves of nc-SiC were calculated (Ivashchenko, 2007). So far, to our knowledge, comprehensive theoretical studies on the mechanical properties of boron, carbon or nitrogen doped nanocrystalline SiC are still lacking.

Different from the previous modeling approach (Shen and Atluri, 2004; Ma etc. 2006; Raghavan and Ghosh,2004; Kadowaki and Liu, 2005; Yang and Tewary, 2006), this paper is concerned with application of the newly formulated atomistic field theory (AFT) (Chen,2005,2006a,b,c,d,2008) for nanocrystalline boron-, boron/nitrogen- and silicon/nitrogen- doped silicon carbide materials systems (B-, BN- and SiN-SiC). The main goal of this work is to investigate the atomic scale properties and behaviors. We are particularly interested in the effects of composition of grain boundaries on the mechanical properties of nc-SiC. General framework of AFT and its finite element implementations are briefly introduced in section 2. Simulation results of nanocrystalline silicon carbide are presented in section 3. We conclude this paper with a brief summary and discussions in section 4.

2 General framework of AFT and its finite element implementations

Classical continuum mechanics view a material as a homogenized continuum. A homogeneous material is one having identical properties at all points. This definition is actually dependent on length scale or resolution that one is concerned. At macroscopic scale, when the resolution is in the range of meters, even polycrystalline materials can be considered as homogeneous materials. However, at nano scale, even a single crystalline material may not be homogeneous, for example, multi-element materials like SiC, SiO_2, etc, because properties, such as mass density, are not identical at any point; stresses or strains evaluated at each atom would be different from that evaluated at unit cell level. Therefore, an atomistic system is not a homogeneous material at atomic/nano scale. We believe that it is necessary to include additional internal variables and additional inhomogeneous fluxes to represent an atomistic multi-element system. This has been analytically proved through the formulation of AFT, and is consistent with the ideas of some micro-continuum theories such as Micromorphic theory (Eringen, 1964), Microstructure theory (Mindlin, 1964), Micropolar theory (Eringen, 1965) and Cosserat theory (Cosserat, 1965), all of which assume the local atomic bonding unit, i.e., the smallest structural unit, as an inner or microscale structure. In the molecular dynamics simulation originated from many body dynamics, only the motions of discrete atoms are considered. As a consequence, MD is well suitable for the modeling of materials behavior at atomic scale but limited in the length and time scale. As an ex-

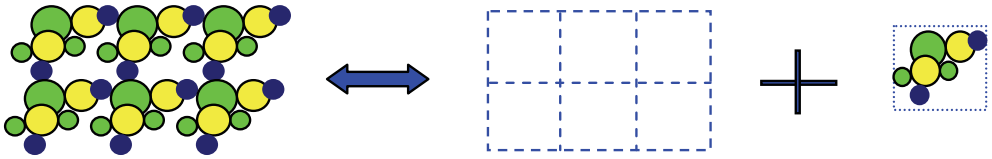

Figure 1: Atomistic view of crystal structure: Crystal structure = lattice + local atomic bonding units

tension of the micromorphic theory and molecular dynamics, in the AFT, there is still continuous lattice deformation but discrete internal deformation. Therefore, the basic set up of AFT is to decompose the deformation of the crystalline solids into continuous lattice deformation and discrete internal deformation shown as Fig.1.

Microscopic dynamic quantities are functions of phase-space coordinates $(\mathbf{r},\mathbf{p})$, i.e., the positions and momenta of atoms. In physical space, the local density of any measurable phase-space function $A(\mathbf{r},\mathbf{p})$ can generally be defined as

$$\begin{aligned}&\mathbf{A}(\mathbf{x},\mathbf{y}^{\alpha},t)\\&=\sum_{k=1}^{n}\sum_{\xi=1}^{\nu}A\{\mathbf{r}(t),\mathbf{p}(t)\}\delta(\mathbf{R}^{k}-\mathbf{x})\tilde{\delta}(\Delta\mathbf{r}^{k\xi}-\mathbf{y}^{\alpha})\\&\equiv\mathbf{A}^{\alpha}(\mathbf{x},t),\end{aligned}\tag{1}$$

Here, k and ξ are the indices for unit cells and atoms within each unit cell. The first delta function is a localization function that provides the link between phase space and continuous physical space descriptions. It can be a Dirac δ-function (Irvine and Kirkwood, 1950), or a distribution function (Hardy, 1982) with normalized conditions. The second delta function is a sharp localization function that identifies $\mathbf{y}^{\alpha}$ to be $\Delta\mathbf{r}^{k\alpha}$.

For simulations at atomic scale, to smooth out the results and to obtain results close to experiments, measurements of physical quantities are necessary to be collected and averaged over finite time duration. Therefore, in deriving the field description of atomic quantities and balance equations of AFT, it is the time-interval averaged quantities that are used, and the time-interval averaged (at time t in the interval Δt) local density function takes the form

$$\begin{aligned}\overline{A}^{\alpha}(\mathbf{x},t)=\langle A^{\alpha}\rangle&\equiv\frac{1}{\Delta t}\int_{0}^{\Delta t}A^{\alpha}(\mathbf{x},t+\tau)d\tau\\&=\frac{1}{\Delta t}\int_{0}^{\Delta t}\sum_{k=1}^{n}A\left(\mathbf{r}(t+\tau),\mathbf{p}(t+\tau)\right)\delta(\mathbf{R}^{k}-\mathbf{x})\\&\quad\tilde{\delta}(\Delta\mathbf{r}^{k\alpha}-\mathbf{y}^{\alpha})d\tau.\end{aligned}\tag{2}$$

Following the definitions presented by Chen and her coworkers (Chen, 2003a), the continuous local average physical quantities including mass density, linear momentum density, internal force density, temperature and external force density can be defined as following:

$$\overline{\rho}^{\alpha}(\mathbf{x},t)=\overline{\rho}(\mathbf{x},\mathbf{y}^{\alpha},t)=\left\langle\sum_{k=1}^{n}m^{\alpha}\delta(\mathbf{R}^{k}-\mathbf{x})\tilde{\delta}(\Delta\mathbf{r}^{k\alpha}-\mathbf{y}^{\alpha})\right\rangle,\tag{3}$$

$$\overline{\rho}^{\alpha}(\overline{v}+\Delta\overline{v}^{\alpha})=\left\langle\sum_{k=1}^{n}m^{\alpha}(\mathbf{V}^{k}+\Delta v^{k\alpha})\delta(\mathbf{R}^{k}-x)\tilde{\delta}(\Delta\mathbf{r}^{k\alpha}-y^{\alpha})\right\rangle,\tag{4}$$

$$\overline{\mathbf{f}}^{\alpha}_{\mathrm{int}}(\mathbf{x})\equiv\left\langle\sum_{k=1}^{n}\left(\sum_{l=1}^{n}\sum_{\beta=1}^{\nu}\mathbf{f}_{1}^{l\beta\,k\alpha}+\sum_{\beta=1}^{\nu}\mathbf{f}_{2}^{k\alpha}\right)\delta(\mathbf{R}^{k}-\mathbf{x})\tilde{\delta}(\Delta\mathbf{r}^{k\alpha}-\mathbf{y}^{\alpha})\right\rangle.\tag{5}$$

$$T^{\alpha}(x)=\left\langle\frac{\Delta V}{3k_{B}}\sum_{k=1}^{n}m^{\alpha}(\tilde{\mathbf{V}}^{k\alpha})^{2}\delta(\mathbf{R}^{k}-x)\tilde{\delta}(\Delta\mathbf{r}^{k\alpha}-\mathbf{y}^{\alpha})\right\rangle,\tag{6}$$

$$\overline{f}^{\alpha}_{\text{ext}} \equiv \left\langle \sum_{k=1}^{n} \mathbf{f}_3^{k\alpha} \delta(\mathbf{R}^k - x) \tilde{\delta}(\Delta\mathbf{r}^{k\alpha} - y^{\alpha}) \right\rangle, \quad (7)$$

where $\tilde{\mathbf{V}}^{k\alpha} = \mathbf{V}^{k\alpha} - \overline{v} - \Delta\overline{v}^{\alpha}$ is the difference between the phase space velocity and the local velocity field, k_B is Boltzmann constant; and ΔV is the volume that define the density of lattice points, i.e., the volume of a unit cell; $\mathbf{f}_1^{l\beta}{}^{k\alpha}$ represents the interatomic force between (k,α) and (l,β) atoms in two different unit cells with $\mathbf{f}_1^{k\alpha}{}^{l\beta} = -\mathbf{f}_1^{l\beta}{}^{k\alpha}$; $\mathbf{f}_2^{k\beta}{}^{k\alpha}$ the interatomic force between (k,α) and (k,β) atoms in the same unit cell with $\mathbf{f}_2^{k\alpha}{}^{k\beta} = -\mathbf{f}_2^{k\beta}{}^{k\alpha}$, and $\mathbf{f}_3^{k\alpha}$ represents the body force on atom (k,α) due to the external fields. In this work, it is understood that the summation over $k$and$l$,when $\mathbf{f}_1^{l\beta}{}^{k\alpha}$ is involved, does not include the case $k = l$, and when $\mathbf{f}_2^{k\beta}{}^{k\alpha}$ is involved, the summation over α and β does not include $\alpha = \beta$.

The mathematical representation of conservation equations for averaged mass and balance of linear momentum at atomic scale has been analytically and exactly obtained in terms of averaged field quantities as (Chen, 2003b)

$$\frac{\partial \overline{\rho}^{\alpha}}{\partial t} + \nabla_{\mathbf{x}} \cdot (\overline{\rho}^{\alpha}\overline{\mathbf{v}}) + \nabla_{\mathbf{y}^{\alpha}} \cdot (\overline{\rho}^{\alpha}\Delta\overline{\mathbf{v}}^{\alpha}) = 0, \quad (8)$$

$$\frac{\partial}{\partial t}(\overline{\rho}^{\alpha}(\overline{\mathbf{v}} + \Delta\overline{\mathbf{v}}^{\alpha})) = \nabla_{\mathbf{x}} \cdot [\overline{\mathbf{t}}^{\alpha} - \overline{\rho}^{\alpha}\overline{\mathbf{v}} \otimes (\overline{\mathbf{v}} + \Delta\overline{\mathbf{v}}^{\alpha})] + \nabla_{\mathbf{y}^{\alpha}} \cdot [\overline{\tau}^{\alpha} - \overline{\rho}^{\alpha}\Delta\overline{\mathbf{v}}^{\alpha} \otimes (\overline{\mathbf{v}} + \Delta\overline{\mathbf{v}}^{\alpha})] + \overline{\mathbf{f}}^{\alpha}_{\text{ext}}, \quad (9)$$

where the stress tensor $\overline{t}^{\alpha}$ and $\overline{\tau}^{\alpha}$ are the continuum counterpart of momentum flux density, which is usually defined in terms of a mathematical infinitesimal volume in a homogenized continuum. Corresponding to the decomposition of the deformation of crystalline solids, $\overline{t}^{\alpha}$ and $\overline{\tau}^{\alpha}$ can be represented upon decomposition into a homogeneous part, caused by lattice motion and deformation related to continuum stress, and an inhomogeneous part, caused by internal (relative) atomic motion and deformation. The homogeneous and inhomogeneous kinetic parts are noted as $\overline{\mathbf{t}}^{\alpha}_{\text{kin}}$ and $\overline{\tau}^{\alpha}_{\text{kin}}$. The homogeneous and inhomogeneous potential parts are noted as $\overline{\mathbf{t}}^{\alpha}_{\text{pot}}$ and $\overline{\tau}^{\alpha}_{\text{pot}}$. Mathematically,

$$\overline{t}^{\alpha} = \overline{t}^{\alpha}_{\text{kin}} + \overline{t}^{\alpha}_{\text{pot}} = -\frac{m^{\alpha}}{M}\frac{k_B}{\Delta V}T^{\alpha}\mathbf{I} + \overline{t}^{\alpha}_{\text{pot}} \quad (10)$$

$$\overline{\tau}^{\alpha} = \overline{\tau}^{\alpha}_{\text{kin}} + \overline{\tau}^{\alpha}_{\text{pot}} = -\left(1 - \frac{m^{\alpha}}{M}\right)\frac{k_B}{\Delta V}T^{\alpha}\mathbf{I} + \overline{\tau}^{\alpha}_{\text{pot}} \quad (11)$$

where $M \equiv \sum_{\alpha=1}^{\nu} m^{\alpha}$ is the total mass of a unit cell. Analytically, it has been shown that [Chen, 2006b]

$$\nabla_{\mathbf{x}} \cdot \overline{\mathbf{t}}^{\alpha}_{\text{pot}} + \nabla_{\mathbf{y}^{\alpha}} \cdot \overline{\tau}^{\alpha}_{\text{pot}} = \overline{f}^{\alpha}_{\text{int}}, \quad (12)$$

With equation (2-10), (2-11) and (2-12), equation (2-9) can be rewritten as

$$\overline{\rho}^{\alpha}\frac{d}{dt}(\overline{\mathbf{v}} + \Delta\overline{\mathbf{v}}^{\alpha}) + \frac{m^{\alpha}k_B}{M\Delta V}\nabla_{\mathbf{x}}T^{\alpha} = \overline{\mathbf{f}}^{\alpha}_{\text{int}} + \overline{\mathbf{f}}^{\alpha}_{\text{ext}} \quad (13)$$

For systems with given temperature, i.e., homogeneous temperature field or a steady state temperature field with a constant temperature gradient, equation (2-13) can serve as the governing equations for time-interval averaged atomic displacements, i.e.,

$$\overline{\rho}^{\alpha}\ddot{\overline{\mathbf{u}}}^{\alpha}(\mathbf{x}) = \overline{\mathbf{f}}^{\alpha}_{\text{int}}(\mathbf{x}) + \overline{\mathbf{f}}^{\alpha}_{\text{ext}} + \overline{\mathbf{f}}^{\alpha}_{\text{tem}} \equiv \overline{\mathbf{f}}^{\alpha}_{\text{int}}(\mathbf{x}) + \overline{\mathbf{f}}^{\alpha}, \quad (14)$$

where $\overline{\mathbf{u}}^{\alpha}(\mathbf{x})$ is the displacement of α-th atom embedded within a material point $\mathbf{x}$, $\overline{\mathbf{f}}^{\alpha}$ is the density of the force acting on the $\alpha - th$ atom due to the external force and temperature field. Generally, $\overline{\mathbf{f}}^{\alpha}_{\text{int}}$ is a nonlocal and nonlinear function of averaged atomic displacements or positions, and can be obtained through fitting to experimental measurements or first principle calculations. In general, it can be expressed as

$$\overline{\mathbf{f}}^{\alpha}_{\text{int}} = \int_{\Omega(\mathbf{x}')}\int_{\Omega(\mathbf{x}'')} \sum_{\beta=1}^{\upsilon}\sum_{\gamma=1}^{\upsilon} \mathbf{f}\left(\overline{\mathbf{u}}^{\alpha}(\mathbf{x}), \overline{\mathbf{u}}^{\beta}(\mathbf{x}'), \overline{\mathbf{u}}^{\gamma}(\mathbf{x}'')\right) d\mathbf{x}' d\mathbf{x}''. \quad (15)$$

In this paper, for covalent nanocrystalline SiC materials, $\overline{\mathbf{f}}^{\alpha}_{\text{int}}$ is derived from the three-body interatomic potential in Tersoff form (Tersoff, 1989). Note that eq. (2-14) is the balance equation that is in terms of field variable, i.e., displacement

field, and local internal force density. This gives us the opportunity to use different resolutions to measure the continuous distributed local densities. Following the standard procedure of finite element method (FEM), we can use shape functions to eliminate a majority of degree of freedom by seeking an approximate displacement field for each atom, i.e.,

$$\hat{\mathbf{u}}^{\alpha}(\mathbf{x}) = \mathbf{\Phi}_{\xi}(\mathbf{x}) U_{\xi}^{\alpha}, \text{ or } \hat{u}_{i}^{\alpha}(\mathbf{x}) = \Phi_{i\xi}(\mathbf{x}) U_{\xi}^{\alpha}, \quad \xi = 1,2,\ldots,n, \quad (16)$$

where n is the number of all unknown parameters in the approximation function, and $\hat{\mathbf{u}}^{\alpha}(\mathbf{x})$stands for the approximate displacement of the α-th atom within an element if finite element method is used. The weak form of eq. (2-14) can be obtained by weighted residual method:

$$\int_{\Omega(\mathbf{x})} \mathbf{\Phi}_{\eta} \Bigg(\overline{\rho}^{\alpha} \ddot{\overline{\mathbf{u}}}^{\alpha}(\mathbf{x}) - \int_{\Omega(\mathbf{x}')} \int_{\Omega(\mathbf{x}'')} \sum_{\beta=1}^{\upsilon} \sum_{\gamma=1}^{\upsilon} \mathbf{f}\left(\overline{\mathbf{u}}^{\alpha}(\mathbf{x}), \overline{\mathbf{u}}^{\beta}(\mathbf{x}'), \overline{\mathbf{u}}^{\gamma}(\mathbf{x}'') \right) d\mathbf{x}' d\mathbf{x}'' - \overline{\mathbf{f}}^{\alpha} \Bigg) d\mathbf{x} = 0, \quad (17)$$

i.e.,

$$\begin{aligned} &\int_{\Omega(\mathbf{x})} \overline{\rho}^{\alpha} \mathbf{\Phi}_{\eta}(x) \mathbf{\Phi}_{\xi}(x) \ddot{U}_{\xi}^{\alpha} d\mathbf{x} \\ &- \int_{\Omega(\mathbf{x})} \int_{\Omega(\mathbf{x}')} \int_{\Omega(\mathbf{x}'')} \mathbf{\Phi}_{\eta}(x) \sum_{\beta=1}^{\upsilon} \sum_{\gamma=1}^{\upsilon} \mathbf{f}\Big(\mathbf{\Phi}_{\xi}(x) U_{\xi}^{\alpha}, \mathbf{\Phi}_{\xi}\left(x'\right) U_{\xi}^{\beta}, \mathbf{\Phi}_{\xi}\left(x''\right) U_{\xi}^{\gamma} \Big) d\mathbf{x} d\mathbf{x}' d\mathbf{x}'' \\ &- \int_{\Omega(\mathbf{x})} \mathbf{\Phi}_{\eta}(x) \overline{f}^{\alpha} d\mathbf{x} = 0, \end{aligned} \quad (18)$$

the matrix form of equation (2-18) is

$$M\ddot{U} = F_{\text{int}}(U) + F. \quad (19)$$

Since AFT has been constructed in terms of local densities, in the finite element implementation of AFT, different meshes can be used in regions of different concerns. For regions where the materials deform collaboratively, coarse mesh (Element Length = $n \times$ Lattice Constant) can be employed (Xiong, 2008), the degree of freedoms can be largely eliminated and the computational cost can be reduced. For the material with highly localized deformation, finest mesh (Element Length = Lattice Constant) can be used. By this way, the connectivity of the finite element mesh is defined by the network of lattice points, and the computational model will be naturally reduced to an atomic-scale model. Then the material behaviors at atomic scale can be simulated (Xiong, 2007a,b). In this work, we mainly discussed the numerical results in which finest mesh has been employed.

2.1 Modeling and Simulation of nanocrystalline B-, BN- and SiN-SiC under Tension

Numerically, columnar grain structure is commonly used in the modeling of nanocrystaline materials since it is well established in the literature (Yamakov, 2001, 2003) as a means of studying deformation mechanisms of nanomaterial behavior in a computationally efficient manner. Experimentally, thin ceramic films composed of extremely small (3∼5 nm) grains and atom-wide GBs (∼0.2 nm wide) can now be produced using plasma-enhanced chemical vapor deposition techniques (Xiao, 2004). Therefore, for feasibility and efficiency, the computational nanocrystalline SiC model carried out in this study is in a thin film form with dimension of 12 nm ×12 nm ×1.5 nm in 3-D space (coordinate noted as x, y and z in Fig.2a) and with ultrafine columnar grains, mean diameter of which is $d \approx 3-4$ nm. After the atomistic computational model is constructed (Fig.1a), the finest finite element mesh can be generated with the nodes coinciding with the centers of each complete or incomplete unit cell (Fig.1b). There are 5043 nodes and 3200 elements in the computational model (Fig.2b) of 4×10^4 atoms. A displacement controlled tensile loading (constant velocity of $v \approx 1280$ m/sec, Fig.2c,d) is then applied along y direction.

In experiments, structure information in nanocrystalline microstructure especially the local information in the grain boundaries is not

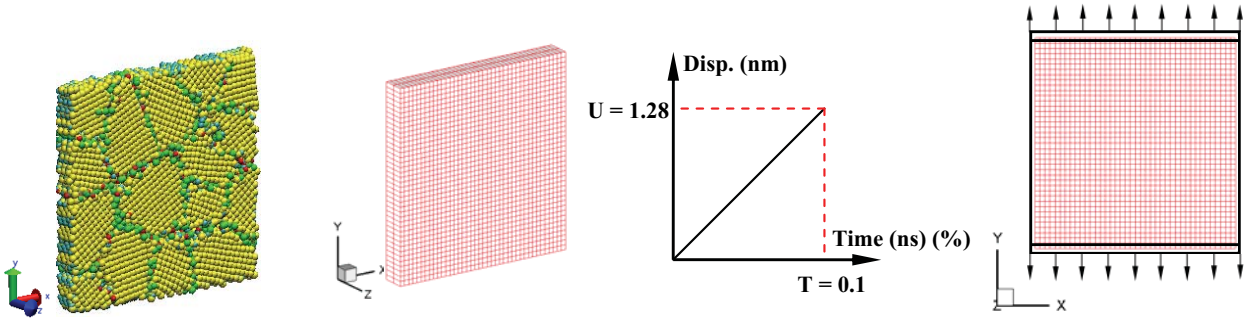

(a) Computational Sample **(b) Finite Element Mesh** **(c) Loading History** **(d) Boundary Conditions**

Figure 2: Computational Model

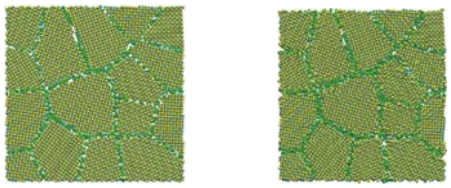

(1) Initial atomic configuration **(2) Relaxed atomic configuration**

(a) Relaxation of B-SiC specimen

(1) Initial atomic configuration **(2) Relaxed atomic configuration** **(1) Initial atomic configuration** **(2) Relaxed atomic configuration**

(b) Relaxation of BN-SiC specimen **(c) Relaxation of SiN-SiC specimen**

Figure 3: Atomic configuration for the relaxation of nanocrystalline SiC

readily available, such as HRTEM, which provide only average structural information on these highly inhomogeneous materials. Therefore, the first objective of this work is to develop a structural model for nanocrystalline SiC.

Fully dense nanocrystalline virtual sample of doped SiC are first assembled using Voronoi construction (Voronoi, 1908). The polyhedral grains are filled with atoms according to the specific misorientation angle assigned to each grain. The initial locations of the grain seeds are randomly distributed. With the grain interiors remaining completely impurity free, substitution solute atoms are then incorporated into the sample by replacing a certain percentage of host atoms (Si or C) in the grain boundaries with various doping concentration. Similar with what has been reported in the simulations of doped nanocrystalline copper (Millett, 2006). By initially placing the dopant atoms in the interfacial regions, the segregation process, which is slow and diffusional and beyond the time scales attainable atomistic simulations, is by passed. Then equation (2-19) is integrated to find the grain boundary structures at thermodynamic and mechanical equilibrium for the entire specimen with zero ambient stress and a given homogeneous temperature field T = 300K. This process is generally referred as relaxation of the forces and stresses in atomistic simulation. For the specimen with average grain size $d \approx 3$ nm and boron, boron/nitrogen or silicon/nitrogen dopants in the GBs, the microstructures and stress distributions before and after the relaxations are shown in Fig.3 and Fig.4.

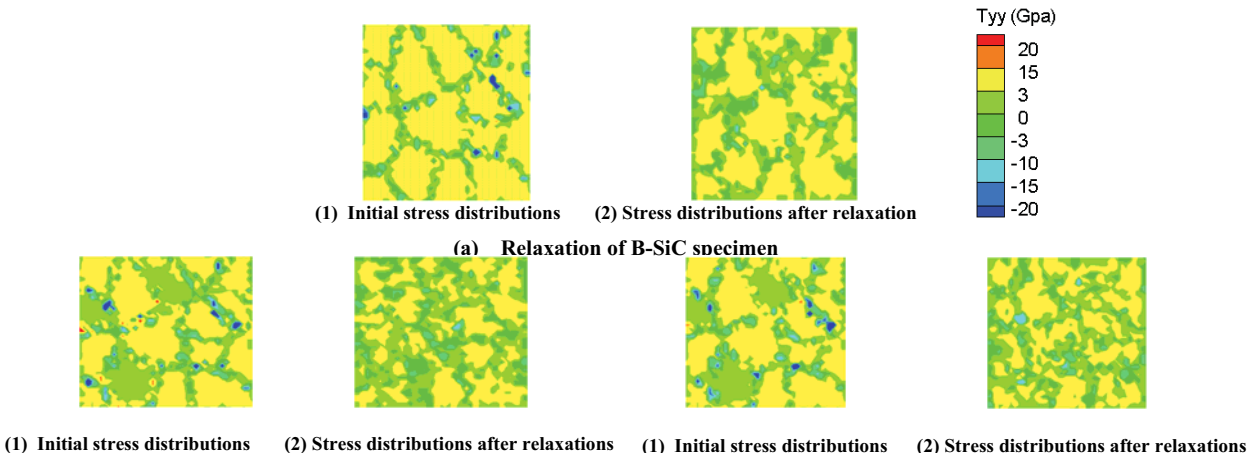

Figure 4: Stress (σ_{22}) distributions for the relaxation of nanocrystalline SiC

In general, the avoidance of significant grain growth in nanophase SiC is extremely difficult compared with some other nanophase ceramics such as TiCN. However, from the atomic configuration shown in Figure 1, it is seen that the formation of amorphous phase in the GBs through doping insoluble elements (boron, nitrogen or silicon) is an efficient way of restricting grain growth. We see two types of atoms in the obtained nanocrystalline structure: (1) atoms with normal coordination number in the crystalline grains; (2) atoms forming the disordered IGFs in the GBs.

From Fig.3, it is found that different dopants have resulted in different porosity and incomplete bonding GBs. Obviously, the IGFs with silicon nitrogen additive (Fig.3c) are thicker and have a higher porosity than that with boron/nitrogen additive (Fig.3b), while the IGFs in the specimen with boron additive (Fig.3a) are relatively dense. It should be emphasized that both the porosity and thickness of IGFs can mask or distort the material properties, and are of utmost importance, especially in understanding the mechanism of mechanical behavior in nanocrystalline SiC ceramics.

Local stress distributions before and after the relaxation are plotted in Fig.4. It is observed that there is a heterogeneous stress field over the specimen although it has reached thermal mechanical equilibrium through the relaxation. There exists residual tensile stress in the interior of crystalline SiC grains and compressive stress in the GBs. In some cases (Fig.4b and Fig.4c), the stress variations in the GBs can extend deep into neighboring grains.

The stress-strain curves of specimen with different dopants are shown in Fig.5. It is shown in Fig.5a that the stress-strain curve of B-SiC exhibits five characteristic regimes: (1) Regime 1 is entirely elastic and ends at $\varepsilon = 0.025$. In this regime, deformations of both the crystalline SiC and GBs are elastic and reversible. The constitutive response is, therefore, a combination response of elastic deformation of crystalline SiC and amorphous boron GBs. As a result of the combination of the deformation mechanisms, the Young's modulus is $E_1 \approx 400$ GPa, which is between experimental value $E \approx 450$ GPa for SiC and $E \approx 230$ GPa for boron (Ding, 2006); (2) Regime 2 is an elastic shoulder which extends from $\varepsilon = 0.025$ to $\varepsilon = 0.04$. A crossover of deformation mechanisms occurs in this regime. The crystalline SiC was gradually unloaded but the GBs are still in loading since the "cementlike" GBs are still trying to hold the grains together; (3) Regime 3 starts when crystalline SiC grains are almost fully unloaded and the GBs continue to be loaded until $\varepsilon = 0.061$. In this regime, boron GBs are still in elastic deformation and the corresponding tangent modulus is $E_2 \approx 220$ GPa, which is in the same order with experimental value $E \approx 230$ GPa for boron at nanoscale (Ding, 2006); (4) In regime 4, the GBs begin to yield, and the plastic behavior is accommo-

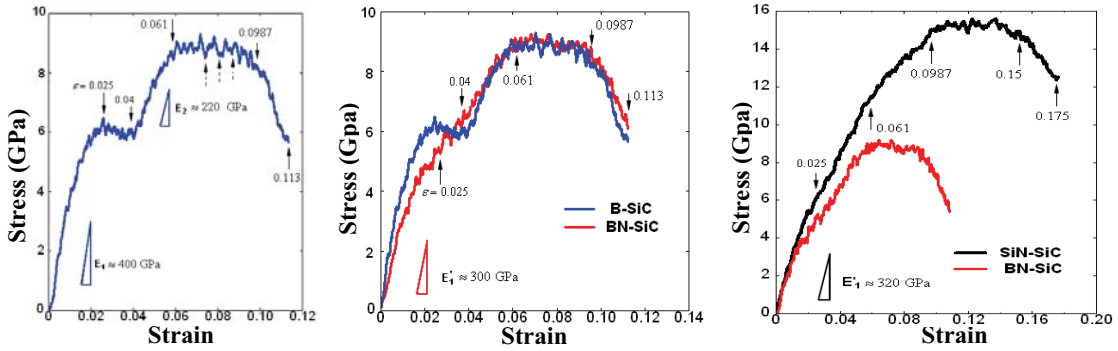

Figure 5: Stress-strain curves of nanocrystalline SiC thin film under tension

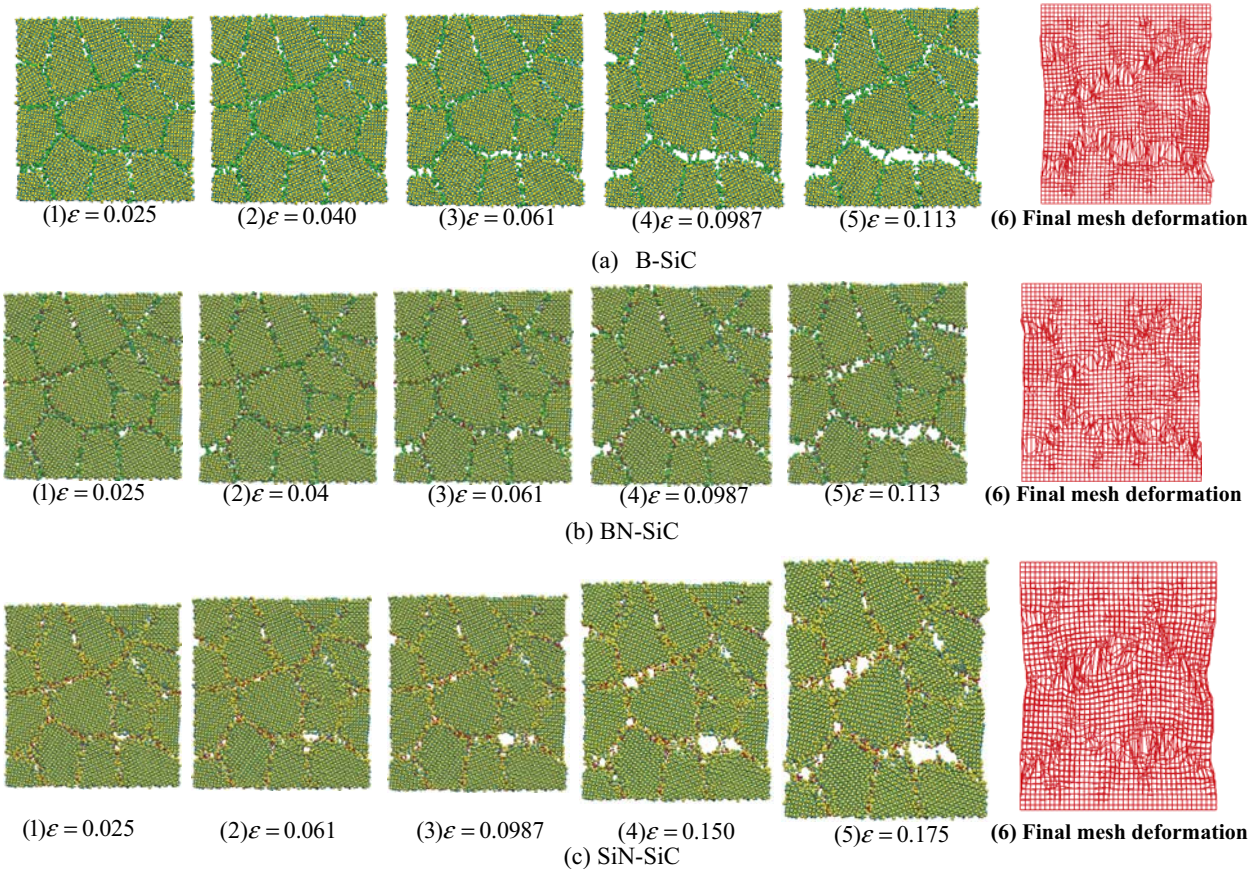

Figure 6: Atomic arrangements and mesh deformations of nanocrystalline SiC thin film under tension

dated by amorphous phase. Grains are beginning to decouple from one another gradually (Fig.6-a3∼a4). It should be noticed that this plastic regime contains a series of periodic stress drops (dashed arrows in Fig.5a). These periodic drops are believed to be related to dislocation activities. Similar phenomena has been observed elsewhere (Priya,2006; Xiong, 2007b);(5) Tensile failure occurs at a critical strain of 0.0987 in regime 5. Applying a small increment strain beyond this critical point causes a dramatic stress reduction. Intergranular crack has been formed (Fig.6-a5), and the specimen cannot sustain further tensile elongation.

Compared with B-SiC, BN-SiC and SiN-SiC exhibit totally different constitutive response

(Fig.5b∼c). Although more nano-sized pores have been observed in triple junctions of the grains when silicon nitrogen are doped (Fig.3c), the stress-strain curves in Fig.5b-c show that the failure strain of SiN-SiC is about $\varepsilon = 0.15$ and the strength is$\sigma_{UTS} \approx 16$ GPa. Both are about 40% higher than those of B-SiC and BN-SiC. Corresponding atomic arrangements and mesh deformations are shown in Fig.6a-c. The mesh deformations of all three cases show that the deformations of nanocrystalline SiC mainly localized in the GBs (Fig.6-a6∼c6). However, highest ductility has been observed in SiN-SiC (Fig.6-c5).

2.2 Summary and discussion

In this paper, the general framework and the basic set ups of an atomistic field theory (AFT) and its finite element formulations have been introduced. In terms of local averaged physical quantities, mathematically, it has been shown that the general principles of AFT are valid at both atomic and continuum level. As a continuum field theory, AFT consists of two essential parts: the *balance laws* and the *constitutive relations*, with which the dynamic behavior of a material system under a given external field and properly imposed boundary and initial conditions can be uniquely and completely determined. Since the balance equations are valid at the atomic scale, this means that they can be used to solve for atomic displacements, to produce atomic trajectories, and hence to investigate phenomena and properties that originated at the atomic scale.

Since AFT has been constructed in terms of local densities, in the finite element implementations of AFT, different meshes can be used in regions for different concerns. When coarse mesh is used, the degree of freedoms can be largely eliminated and the computational cost can be reduced (Xiong, 2008). When finest mesh is used, i.e., the connectivity of the finite element mesh is defined by the network of lattice points, and AFT will naturally reduce to an atomistic simulation. In this work, we have mainly discussed the numerical results in which the finest mesh has been employed.

Computer simulations of nanocrystalline silicon carbide are performed based on AFT to investigate the effects of the dopants on the mechanical properties. Major findings are summarized as follows: (1) Intergranular glassy amorphous film and nano-sized pores exist in triple junctions of the grains, and there are residual tensile stress in the interior of the crystalline grains and compressive stress in the GBs; (2) Constitutive response of 5 wt% boron doped nanocrystalline SiC exhibits five characteristic regimes: (a) Combination of elastic deformation of crystalline SiC and amorphous boron GBs; (b) Crossover of deformation mechanisms occurs when the crystalline SiC grains are unloaded; (c) Elastic deformation of GBs; (d) Plastic deformations of GBs; (e) Failure; (3) Under tensile loading, comparisons of the mechanical properties of B-SiC, BN-SiC and SIN-SiC show that SiN-SiC exhibits the highest strength, although there are more nano-sized pores in triple junctions of the grains of such specimen.

Acknowledgement: Support from National Science Foundation under Award Numbers CMMI-0646674 is gratefully acknowledged.

References

Chen, D.; Zhang, X.; Ritchie, R.O. (2000): Effects of Grain-Boundary Structure on the Strength, Toughness, and Cyclic-Fatigue Properties of a Monolithic Silicon Carbide, *Journal of the American Ceramic Society* vol. 83, 2079-2081

Chen, Y.; Lee, J.D. (2003a): Connecting molecular dynamics to micromorphic theory Part I: Instantaneous mechanical variables, *Physica A* vol. 322, 359-376.

Chen, Y.; Lee, J.D. (2003b): Connecting molecular dynamics to micromorphic theory Part II: Balance laws, *Physica A* vol. 322, 377-392.

Chen, Y.; Lee, J.D. (2005): Atomistic Formulation of a Multiscale Theory for Nano/Micro Physics, *Philosophical Magazine* vol.85, 4095-4126.

Chen, Y.; Lee, J.D.; Lei, Y.; Xiong, L. (2006a): A Multiscale Field Theory: Nano/Micro Materials, G. C. Sih (Eds), Book chapter (invited contribution) on *Multiscaling in Molecular and Contin-*

uum Mechanics, Springer,23-65.

Chen, Y. (2006b): Local stress and heat flux in atomistic systems involving three-body forces, *Journal of Chemical Physics* vol.124, 054113-1.

Chen, Y.; Lee,J.D. (2006c): Conservation laws at nano/micro scales, *Journal of Mechanics of Materials and Structures* vol.1, 681-704.

Chen, Y.; Lee, J.D.; Xiong,L. (2006d): Stresses and strains at nano/micro scales, *Journal of Mechanics of Materials and Structures* vol.1, 705-724.

Chen, Y.; Lee, J.D.; Xiong,L. (2008): Heat Flux at nano/micro scales, *Journal of Heat Transfer*, accepted for publication.

Cosserat, E. (1909): *Theorie des corps deformable*, Hermann, Paris.

Ding, W.; Lorenzo, C.; Chen, X.; Kohlhaas, K.M.; Ruff, R.S. (2006): Mechanics of crystalline boron nanowires, *Composites Science and Technology* vol. 66, 1112-1124.

Eringen, A.C.; Suhubi, E.S. (1964): Nonlinear theory of simple micro-elastic solids–I, *International Journal of Engineering Science* vol. 2, 189-200.

Eringen, A.C. (1965): *Theory of micropolar continua, Developments in Mechanics,* T.C.Huang and M.W.Johnson, Jr. (Eds). *Vol. 3*, Wiley, New York.

Hardy, R.J. (1982): Formulas for determining local properties in molecular-dynamics simulations: Shock waves, *Journal of Chemical Physics* vol.76(1), 622-628.

Irvine, J.H.; Kirkwood, J.G. (1950): The statistical theory of transport processes. IV. The equations of hydrodynamics, *Journal of Chemical Physics* vol.**18**, 817-829.

Ivashchenko, V.I.; Turchi, P.E.A.; Shevchenko, V.I. (2007): Simulations of the mechanical properties of crystalline, nanocrystalline, and amorphous SiC and Si, *Physical Review B* vol. 75, 085209.

Kadowaki, H.; Liu, W.K. (2005): A multiscale approach for the micropolar continuum model, *CMES: Computer Modeling in Engineering and Science* vol.7,269-282

Kim, Y.W.; Chun, Y.S.; Nishimura, T.; Mitomo, M.; Lee, Y.H. (2007): High-temperature strength of slicon carbide ceramics sintered with rare-earth oxide and aluminum nitride, *Acta Materialia* vol. 55, 727-736.

Keblinsky, P.; Phillpot, S.R.; Wolf, D.; Gleiter, H. (1996): Thermodynamics criterion for the stability of amorphous intergranular films in covalent materials, *Physical Review Letter* vol.77, 2965-2968.

Liao, F.; Girshick, S.L.; Mook, W.M.; Gerberich, W.W. (2005): Superhard nanocrystalline silicon carbide films, *Applied Physics Letter* vol. 86, 171913.

Ma, J.; Lu, H.; Wang, B.; Hornung, R.; Wissink, A.; Komanduri, R. (2006): Multiscale Simulation Using Generalized Interpolation Material Point (GIMP) Method and Molecular Dynamics (MD), *CMES: Computer Modeling in Engineering & Sciences*, vol. 14 (2), 101-118

Madar, R. (2004): Materials science: Silicon carbide in contention, *Nature* vol.430, 974-975.

Millett, P.C.; Selvam, R.P.; Saxena,A. (2006): Molecular dynamics simulations of grain size stabilization in nanocrystalline materials by addition of dopants, *Acta Materialia* vol.54, 297-303.

Mindlin, R.D. (1964): Microstructure in linear elasticity, *Arch. Rat. Mech. Anal.* vol.**16** 51-78.

Mo, Y.; Szlufarska, I. (2007): Simultabeous enhancement of toughness, ductility, and strength of nanocrystalliine ceramics at high strain-rates, *Applied Physics Letters* vol.90, 181926.

Raghavan, P.; Ghosh, S. (2004): Adaptive multiscale computational modeling of composite materials, *CMES: Computer Modeling in Engineering and Science* vol.5, 151-170

Shen, S.; Atluri, S.N. (2004): Multiscale simulation based on the meshless local Petrov-Galerkin (MLPG) method, *CMES: Computer Modeling in Engineering & Sciences* 5 vol. (3), 235-255

Shen, S.; Atluri, S.N. (2004): Computational nano-mechanics and multi-scale simulation, *CMC: Computers, Materials & Continua* 1 vol. (1), 59-90

Shen, S.; Atluri, S.N. (2004): Atomic-level

stress calculation and continuum-molecular system equivalence , *CMES: Computer Modeling in Engineering & Sciences* vol. 6 (1), 91-104

Shinnoda, Y.; Yoshida, M.; Akatsu, T.; Wakai, F. (2004): Compression deformation mechanism of silicon carbide: fine-grained boron- and carbon-doped silicon carbide fabricated by hot isostatic pressing, *Journal of the American Ceramic Society* vol. 87 [10], 1919-1926.

Szlufarska, I.; Nakano, A.; Vashishta,P. (2005): A crossover in the mechanical response of nanocrystalline ceramics, *Science* vol.309, 911-914.

Tang, M.; Yip, S. (1994): Lattice instability in β-SiC and simulation of brittle fracture, *Journal of Applied Physics* vol. 76, 2719-2725.

Tang, M.; Yip, S. (1995): Atomistic simulation of thermomechanical properties of β-SiC, *Physical Review B* vol.52, 15150-15159.

Tersoff, J. (1989): Modeling solid-state chemistry: Interatomic potentials for multicomponent systems, *Physical Review B* vol.31, R5566-5568.

Vashishta, P.; Kalia, R.K.; Nakano, A. (2006): Multimillion atom simulations of dynamics of oxidation of an aluminum nanoparticles and nanoindentation on ceramics, *Jounal of Physical Chemistry.B* vol.110, 3727-3733.

Voronoi, G.Z. (1908): Nouvelles applications des paramtres continus s la thorie des. Formes quadratiques, deuxime mmoire, *Journal fur die Reine und Angewandte Mathematik,* vol.134, 198-287

Xiong, L.; Chen, Y.; Lee, J.D. (2007a): Atomistic simulation of mechanical properties of diamond and silicon carbide by a field theory, *Modeling and Simulation in Material Science Engineering* vol.15, 535-551.

Xiong, L.; Chen, Y.; Lee, J.D. (2007b): Simulation of Dislocation Nucleation and Motion in single Crystal Magnesium Oxide by a Field Theory, *Computational Material Science*, in press.

Xiong,L.; Chen,Y.; Lee, J.D. (2008): Modeling and simulation of MgO from atoms to continuu, *International Journal of Solids and Structures*, preparing for submission.

Xiao, X.; Birrell, J.; Gerbi, J.E.; Auciello, O.; Carlisle, J.A. (2004): Low temperature growth of ultrananocrystalline diamond, *Journal of Applied Physics* vol. 96, 2232-2239.

Yamakov, V.; Wolf, D.; Salazar, M.; Phillpot, S.R.; Gleiter, H. (2001): Length-scale effects in the nucleation of extended dislocations in nanocrystalline Al by molecular-dynamics simulation, *Acta Materialia* vol. 49, 2713-2722.

Yamakov, V.; Wolf, D.; Phillpot, S.R.; Gleiter,H. (2003): Dislocation-dislocation and dislocationi-twin reactions in nanocrystalline Al by molecular-dynamics simulation, *Nature Materials*, vol.1,45-48

Yamakov, V.; Wolf, D.; Phillpot, S.R.; Gleiter, H. (2003): Dislocation–dislocation and dislocation–twin reactions in nanocrystalline Al by molecular dynamics simulation , *Acta Materialia* vol. 51, 4135-4147

Yang, B.; Tewary, V.K.(2006): Efficient Green's function modeling of line and surface defects in multilayered anisotropic elastic and piezoelectric materials, *CMES: Computer Modeling in Engineering and Science* vol.15, 165-177

Zhang, X.; Sixta, M.E.; Jonghe, L.C.D. (2001): Secondary phases in hot-pressed Aluminum-Boron-Carbon-Silicon Carbide, *Journal of the American Ceramic Society* vol. 84(4), 813-824.

Zhang, X.; Lee, G.Y.; Chen, D.; Ritchie, R.O.; Jonghe, L.C.D. (2003): Abrasive wear behavior of heat-treated ABC-Silicon carbide, *Journal of the American Ceramic Society* vol. 86(8), 1370-1391.

Zhao, Y.; Qian, J.; Luke, L.D.; Cristian, P.; Zhang, J.; Georgiy, A.V.; Zerda, T.W. (2004): Enhancement of fracture toughness in nanostructured diamond-SiC composites, *Applied Physics Letter* vol.84, 1356-1358

Zhou, Y.; Hirao, K.; Toriyama, M.; Yamauchi, Y.; Kanzaki, S. (2001): Effects of intergranular phase chemistry on the microstructure and mechanical properties of silicon carbide ceramics densified with rare-earth oxide and alumina additions, *Journal of the American Ceramic Society* vol. 84 (7), 1642-1644.